THE JOURNAL OF PHYSICAL CHEMISTRY B
A JOURNAL OF THE AMERICAN CHEMICAL SOCIETY

pubs.acs.org/JPCB

Article

Benchmarking Thiolate-Driven Photoswitching of Cyanine Dyes

Lucas Herdly, Peter W. Tinning, Angéline Geiser, Holly Taylor, Gwyn W. Gould, and Sebastian van de Linde*

Cite This: https://doi.org/10.1021/acs.jpcb.2c06872

Read Online

ACCESS | Metrics & More | Article Recommendations | Supporting Information

ABSTRACT: Carbocyanines are among the best performing dyes in single-molecule localization microscopy (SMLM), but their performance critically relies on optimized photoswitching buffers. Here, we study the versatile role of thiols in cyanine photoswitching at varying intensities generated in a single acquisition by a microelectromechanical systems (MEMS) mirror placed in the excitation path. The key metrics we have analyzed as a function of the thiolate concentration are photon budget, on-state and off-state lifetimes and the corresponding impact on image resolution. We show that thiolate acts as a concentration bandpass filter for the maximum achievable resolution and determine a minimum of ∼1 mM is necessary to facilitate SMLM measurements. We also identify a concentration bandwidth of 1−16 mM in which the photoswitching performance can be balanced between high molecular brightness and high off-time to on-time ratios. Furthermore, we monitor the performance of the popular oxygen scavenger system based on glucose and glucose oxidase over time and show simple measures to avoid acidification during prolonged measurements. Finally, the impact of buffer settings is quantitatively tested on the distribution of the glucose transporter protein 4 within the plasma membrane of adipocytes. Our work provides a general strategy for achieving optimal resolution in SMLM with relevance for the development of novel buffers and dyes.

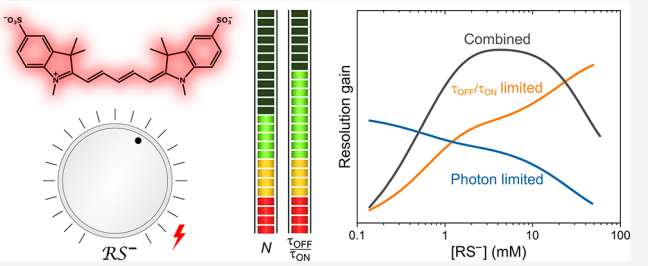

INTRODUCTION

Single-molecule localization microscopy (SMLM) is a powerful super-resolution technique that has become a standard tool for studying biological questions.[1−3] Its key advantages, i.e., sub 20 nm resolution and quantitative imaging of biological structures, is based on the precise control of the employed photoswitches. Therefore, much effort has been made to understand the photophysical and -chemical mechanisms of photoswitching.[4−7]

The use of conventional organic dyes in SMLM usually requires a chemical buffer with redox properties. The first class of dyes with which reliable and highly reversible photoswitching had been reported, were the far-red-emitting carbocyanines Cy5 and Alexa Fluor 647 (AF647).[8,9] Although several other organic dyes such as rhodamine and oxazine dyes have been utilized as photoswitches in adapted chemical buffers,[10−13] carbocyanine dyes still stand out for their high molecular brightness and highly reliable photoswitching performance.[12,14] These two key features have paved the way for the success of stochastic optical reconstruction microscopy (STORM)[15] and direct STORM (dSTORM).[16]

The employed photoswitching buffer usually consists of an enzymatic oxygen scavenger system and a thiol containing reducing agent, such as β-mercaptoethanol (BME) or β-mercaptoethylamine (MEA). The buffer is typically set at moderate alkaline pH to increase the formation of thiolate (RS^-), which not only is a major compound in the creation of metastable dark or off-states[10,13,17] but also plays an important role in the photostabilization of organic dyes.[18]

In their comprehensive study, Gidi et al. describe the thiol-based photoswitching mechanism of red emitting cyanine dyes by two competing reactions, i.e., a photostability and a photoswitching pathway.[19] The starting point is the reduction of Cy5 in its triplet state by RS^- and the generation of a geminate radical pair (GRP) [$Cy5^{-\bullet}$, $RS^{\bullet}$]. Hereinafter, (i) Cy5 is either restored to its ground state through back electron transfer,[18] or (ii) the formation of a thiol adduct through geminate radical combination is taking place (Cy5-RS^-).[19] After formation of the off-state, photoinduced or thermal thiol elimination can regenerate Cy5 into its ground state, thus closing the cycle of photoswitching. In summary, the photoswitching mechanism of carbocyanines allows for (i) high photon fluxes through thiolate mediated photostabilization and (ii) creation of long lasting nonfluorescent off-states. This finally leads to the excellent performance of carbocyanines in SMLM; the detection of bright spots on the wide-field camera guarantees high localization precision[20] and trans-

Received: September 27, 2022
Revised: December 20, 2022

ferring the majority of dyes into their off-state allows for resolving structures with high label densities.

Recently, the importance of homogeneous illumination in SMLM and its impact on single-molecule photoswitching has been demonstrated.[21,22] We have introduced a single microelectromechanical systems (MEMS) micromirror for tunable wide-field illumination in SMLM.[22] The MEMS mirror was implemented in the excitation path of our wide-field setup and used as 2D scanning device of the incoming laser beam. Due to its tunability in frequency and oscillation amplitude, the MEMS mirror could either be used to generate an extremely homogeneous illumination for consistent single-molecule photoswitching over large areas or induce intensity gradients within the field of view (FOV). The latter mode allowed us to study single-molecule photoswitching at varying irradiation intensities within a single SMLM acquisition.[22]

Here, the MEMS mirror is employed to study the photoswitching of AF647 on the single-molecule level by applying a range of different buffer settings, i.e., varying concentrations of MEA and pH values. We show how both parameters can be balanced toward optimal SMLM imaging conditions and characterize the working range of the associated thiolate concentration. Furthermore, we study the performance of the enzymatic oxygen scavenger system by monitoring photoswitching kinetics over prolonged imaging periods and demonstrate how the system can be stabilized when influx of oxygen is prevented.

Finally, we apply our findings by quantitatively imaging the glucose transporter type 4 (GLUT4) in the plasma membrane of adipocytes and show how buffer settings impact data quality. Insulin increases the numbers of GLUT4 molecules on the surface of adipocytes by promoting the exocytosis of GLUT4-containing vesicles from intracellular stores to the plasma membrane.[23] However, recent work has argued that the spatial distribution of GLUT4 within the plasma membrane is also regulated by insulin.[24,25] Studies using dSTORM have suggested that insulin promotes the dispersal of GLUT4 from clusters to monomers, and that this may be an important aspect of GLUT4 regulation.[26,27] There is therefore a pressing need to understand the behavior of molecules such as GLUT4 using SMLM techniques.

Our studies underpin the versatile role of thiols in single-molecule photoswitching, provide a guideline for optimizing SMLM imaging, and support the development of novel imaging buffers and dyes.

METHODS

SMLM Setup. The setup was a single-molecule-sensitive, wide-field microscope equipped with a single MEMS micromirror, which has been previously described in detail.[22] Use of a NA 1.49, 60× oil immersion objective (APON60XOTIRF, Olympus) and ∼1.8× postmagnification (OptoSplit II, Cairn) led to an effective camera pixel size of 122 nm. The fluorescence light was filtered with a zt532/640rpc dichroic mirror (Chroma) and multibandpass filter ZET532/640 (Chroma), and imaged on a EMCCD camera (iXon Life 888, Andor). For all measurements, the central area of the EMCCD camera with 512 × 512 pixels was selected, thus resulting in a total FOV of $(62.5\ \mu m)^2$; the camera was recording 30,000 frames at 20 Hz frame rate, except for the experiments on buffer acidification with 15,000 frames at 10 Hz. Buffer acidification and cell measurements were performed with a refractive beam shaping device to generate a flat-field illumination (piShaper 6_6_VIS, AdlOptica), whereas all other experiments were performed with an active MEMS micromirror. The excitation intensity for the full FOV was measured to 0.48 kW cm^{-2} for single-molecule photoswitching using the MEMS illumination and 0.72 kW cm^{-2} for cell measurements using the piShaper.

Sample Preparation. For preparing single-molecule surfaces, we used the following complementary DNA sequences purchased from Eurogentec, Ltd.: 5-GGGAAT-GCGAATCAAGTAATATAATCAGGC-3, which was biotinylated at the 5′ end, and 5-GCCTGATTATATTACTTG-ATTCGCATTCCC-3, which was modified with AF647 at position 8 via internal labeling. Hybridization to dsDNA was performed by mixing sense and antisense strand at a ratio of 2:1 and incubating overnight at room temperature. Single-molecule surfaces were prepared on the basis of albumin, biotinylated albumin and NeutrAvidin as previously described.[22] The average molecular surface density was determined to 5.0 ± 2.5 molecules μm^{-2} (median ± MAD) by analyzing the obtained localization files in Fiji.[28,29]

3T3-L1 adipocytes that stably express a version of GLUT4 which includes a HA epitope in the exofacial domain that is accessible to antibodies in intact cells only when GLUT4 is at the cell surface were grown and differentiated on Nunc multichambered slides as described.[27] HA-GLUT4-GFP is a well-used reporter for GLUT4 trafficking.[30−32] Adipocytes were incubated in serum-free media for 2 h then fixed with 4% paraformaldehyde (PFA) in PBS for 20 min at room temperature. The samples were quenched with 50 mM NH_4Cl in PBS for 10 min, washed with PBS then incubated in blocking solution (2% BSA with 5% goat serum in PBS) for 30 min prior to incubation with anti-HA antibodies (Covance product MMS 101P, mouse monoclonal HA.11) for 90 min. After washing cells were incubated with AF647 anti-mouse antibodies (1:1000) for 60 min, washed, and then incubated in PBS prior to analysis.

Photoswitching Buffer. The photoswitching buffer was prepared according to previously published protocols with all chemicals purchased from Sigma-Aldrich if not otherwise stated.[22,33] The final enzymatic oxygen scavenger system consisted of 5% (w/v) glucose, 10 U mL^{-1} glucose oxidase, and 200 U mL^{-1} catalase (GOC). Mercaptoethylamine (MEA, purchased as cysteamine hydrochloride) was added to the solution at final concentrations of 10−250 mM as indicated. As MEA is the main buffering component (cf. Figure S5), the pH was adjusted by adding designated amounts of KOH, except for 10 and 50 mM at pH 6.5 where HCl was used. To prepare 1 mL of switching buffer, 500 μL of a 10% (w/v) glucose stem solution, 5 μL of an enzyme stock solution as described,[33] up to 50 μL of a 5 M MEA stock solution prepared in dH_2O, and up to 50 μL 1 M KOH or up to 2 μL 1 M HCl were used; the remaining amount to 1 mL was filled with PBS. If not otherwise stated, then the LabTek chambers (Nunc) were completely filled and sealed with a coverslip on top to avoid further gas exchange and air bubbles.

For the titration curve, a 100 mM MEA solution was prepared in GOC photoswitching buffer as described above (Figure S5). 40 mL of the freshly prepared solution was titrated at room temperature with 1 M KOH, while the pH was monitored by a pH meter (Oakton pH 700). The solution was thoroughly mixed via magnetic stirrer and stir bar.

The thiolate concentration was determined according to the Henderson−Hasselbalch equation:[34]

https://doi.org/10.1021/acs.jpcb.2c06872
J. Phys. Chem. B XXXX, XXX, XXX−XXX

$$[RS^-] = [MEA]_0(1 + 10^{(pK_a - pH)})^{-1} \quad (1)$$

with $[MEA]_0 = [RS^-] + [RSH]$ as the total concentration of thiol used.

For monitoring the time-dependent acidification of the photoswitching buffer, the pH of the solvent in the LabTek chamber was measured using pH indicator strips (pH range 5.0−10.0, MQuant) with a step reading of pH 0.5. Photoswitching buffer was prepared with GOC system and 50 mM MEA and set to pH 7.4 using KOH. Measurement of the pH was done at each time point. Unsealed specimen were filled with 750 μL of switching buffer and imaged with the lid off with data being taken just after adding the buffer (0 h) and 2 and 4 h later. The specimen was not moved between experiments and kept on the microscope. The sealed specimen was prepared in the same way, but the chamber was completely filled and sealed with a coverglass on top. The pH was measured just before sealing and after imaging at 20 h later.

SMLM Data Analysis. The analysis of photoswitching kinetics was performed as previously described,[22] slight modifications are described in the Supporting Information. Fourier ring correlation (FRC) maps were generated using the ImageJ plugin NanoJ SQUIRREL.[35]

The theoretical resolution was determined from the variance of the localization uncertainty Δ_x^2.

$$\Delta_x^2 = \frac{\sigma_a^2}{N}\left(\frac{16}{9} + \frac{8\pi\sigma_a^2 b^2}{a^2 N}\right) \quad (2)$$

with $\sigma_a^2 = \sigma^2 + a/12$ and σ as the standard deviation of the point spread function, a as the camera pixel size, b as background noise, and N as number of detected photons.[36] The precision was calculated as the square root of twice the variance to account for the excess noise of the EMCCD.[36] The theoretical precision was multiplied with 2.355 to obtain the theoretical resolution (Figure 4b, squares). For the data shown in Figure 4, σ was set to 140 nm, a = 120 nm, b^2 = 49 photons; for N two scenarios were used: $N = N_{\tau on}$ and $N = \frac{1}{2}N_{\tau on}$. The former scenario ideally assumed that all photons would be captured within one frame leading to a single localization, whereas the latter refers to a more realistic spot brightness due to uncorrelated fluorescence emission and frame acquisition.

The two-dimensional structural resolution was calculated according to the Nyquist−Shannon sampling theorem.[37]

$$d_{2D} = \frac{2}{\sqrt{n}} \quad (3)$$

with n as the label density. The τ_{off}/τ_{on} ratio was considered as the upper limit for the maximum tolerable density within the diffraction limited region (DLR). The DLR is sometimes considered as the fwhm of the PSF, e.g., 340 nm, which would in principle allow to resolve 11 spots per μm^2. Localization software, however, fails in detection of such a high emitter density even if high density algorithms are used. We therefore used a more conservative approximation of the DLR, i.e., DLR = 1 μm^2, which also allowed to use $n = \tau_{off}/\tau_{on}$ in eq 3 (Figure 4b, circles). In addition, a high density case was considered with 5 spots μm^{-2}.[38]

RESULTS AND DISCUSSION

Impact of Thiol Concentration and pH on Photoswitching. Single-molecule surfaces were prepared in chambered coverslips to study the photoswitching of AF647 under dSTORM conditions.[22] Each chamber was filled with differently adjusted buffers, i.e., ranging pH from 6.5 to 8.5 and MEA concentrations from 10 mM to 250 mM, but utilizing the same enzymatic oxygen scavenging system. For the entire set of measurements, illumination and acquisition parameters were kept constant. Single-molecule photoswitching was studied at different laser intensities within a single FOV. This was achieved by using a certain mode of the MEMS mirror in the excitation path of our setup, thus generating a gradient with maximum laser power in the center while attenuating toward the edges of the FOV.[22] Through this, the average single-molecule fluorescence could be directly related to the excitation intensity, which holds true for excitation below the saturation limit, i.e., in the lower kW cm^{-2} range.[39,40] In addition, it has recently been demonstrated that a reduction of the irradiation intensity of the readout laser toward sub kW cm^{-2} levels has an overall positive effect on single-molecule photoswitching and SMLM image quality.[41,42]

The FOV was segmented into 49 subregions (Figure S1a). For each buffer condition, single-molecule time traces were analyzed according to their on- and off-time intervals, which were used to determine the average lifetime of the fluorescent on and dark off states, τ_{on} and τ_{off}, respectively (Figure S1). In addition, the average detected spot brightness, N_{Det}, i.e., the number of photons detected per molecule and frame, was determined. Figure 1 shows these metrics for three different buffer conditions. Overall, increasing pH and MEA concentration led to an increase of τ_{off} and decrease of τ_{on} and N_{Det}. Consequently, the ratio of the lifetimes, τ_{off}/τ_{on}, which is linked to the achievable resolution,[12,14,43,44] increased as well (Figure 1). These results underpin the importance of the irradiation intensity on the photoswitching metrics, with improved values

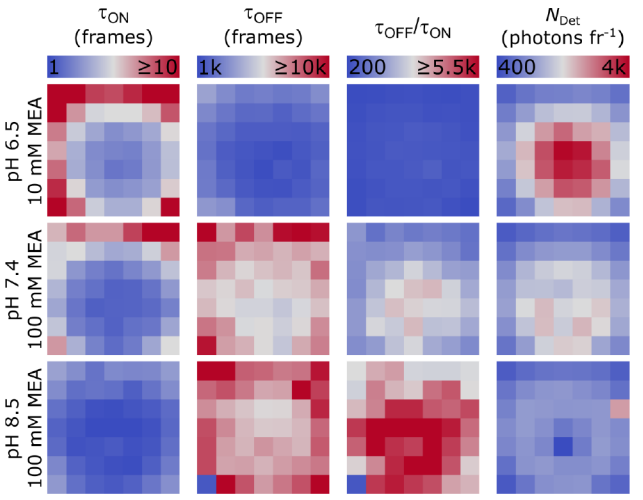

Figure 1. Photoswitching metrics of AF647 for different photoswitching buffer settings with sole illumination at 641 nm employing a MEMS mirror. The entire field of view $(62.5\ \mu m)^2$ was subdivided into 7 × 7 equally sized regions of interest (ROIs). τ_{on}, τ_{off}, τ_{off}/τ_{on}, and N_{Det} are shown for three different buffer settings, i.e., 10 mM MEA at pH 6.5 (upper panel), 100 mM MEA at pH 7.4 (central panel), and 100 mM MEA pH 8.5 (lower panel), all prepared with enzymatic oxygen scavenger system. Note the same scale for each parameter along different buffer settings. One frame corresponds to 50 ms.

https://doi.org/10.1021/acs.jpcb.2c06872
J. Phys. Chem. B XXXX, XXX, XXX−XXX

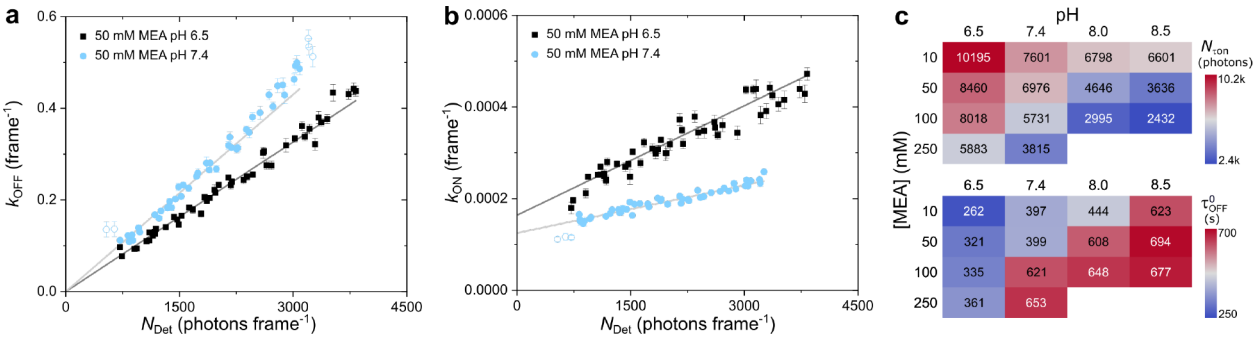

Figure 2. Photoswitching metrics for different buffer settings. a) Linear correlation of the off-switching rate, k_{off}, and the median photon count per spot and frame (N_{Det}, i.e., the spot brightness) for two different buffer settings, i.e., 50 mM MEA pH 6.5 (black) and 50 mM MEA pH 7.4 (blue). The photon budget of the fluorophore (N_{ron}) was determined through the inverse gradient of the linear fit function. b) Linear correlation of the on-switching rate, k_{on}, and N_{Det}. The thermal recovery rate, k^0_{on}, was determined from the nonzero intercept of the fit. a, b) Each data point represents a single ROI as shown in Figure 1. Linear fits to the data are shown as lines in light (pH 7.4) and dark gray (pH 6.5). Error bars are standard errors from data fits. Unfilled circles represent masked data points. One frame corresponds to 50 ms. c) The photon budget N_{ron} (top) and thermal off-state lifetime τ^0_{off} (bottom) for the entire set of MEA concentrations and pH values tested, where $\tau^0_{off} = (k^0_{on})^{-1}$.

toward the center of the FOV, where the laser intensity peaked.

Next, the rate constants at which AF647 is transferred to the off- or on-state, i.e., $k_{off} = \tau_{on}^{-1}$ and $k_{on} = \tau_{off}^{-1}$, respectively, were analyzed as a function of N_{Det} (Figures 2, S2, and S3). Figure 2a shows the expected linear correlation of k_{off} with N_{Det} for two different buffer conditions, i.e., 50 mM MEA at pH 6.5 and pH 7.4. The camera frame rate was chosen to sufficiently sample τ_{on} over a range of excitation intensities, hence distributing the total amount of photons emitted by the fluorophore over several consecutive camera frames. From the inverse gradient of the fit the photon budget of the fluorophore, N_{ron}, was determined, i.e., the total number of photons emitted within τ_{on} (Figures 2a and S2).[22] As can be seen, the gradient of the fit was decreased for pH 6.5, which corresponds to a higher N_{ron} when compared with pH 7.4.

Next, the on-switching rate was studied for different buffer settings. Figure 2b shows the linear increase of k_{on} with N_{Det}, which is linked to the photoinduced repopulation of the ground state of AF647 due to thiol elimination. Restoring fluorescence of AF647 and Cy5 has been previously demonstrated by additional excitation with blue-shifted laser light, e.g., 405, 488, and 514 nm, or solely by the read-out wavelength around 640 nm.[14,16,17,19] The latter approach is usually beneficial because of the lower sensitivity of k_{on} to the red-shifted excitation intensity, which allows for activating small subsets of emitters in a densely labeled sample while the majority remains nonfluorescent. Besides the photoinduced pathway, dissociation of the cyanine-thiol adduct can also occur thermally.[19] Therefore, we determined the thermal recovery rate, k^0_{on}, which could be extracted from the nonzero intercept of the fit as shown in Figure 2b, and finally the thermal off-state lifetime, τ^0_{off}. The change of intercept was already visible for a moderate pH increase, with pH 7.4 leading to a higher τ^0_{off} when compared to pH 6.5. Interestingly, the gradient of the fit was significantly higher for pH 6.5, indicating a higher sensitivity of the recovery rate at this buffer condition.

The photon budgets and thermal off-state lifetimes for different buffer conditions are summarized in Figure 2c. For low pH and MEA concentrations, the photon budgets were higher; an increase in both parameters led to a ~4-fold decrease from 10,200 (10 mM MEA at pH 6.5) to 2,400 photons (100 mM MEA at pH 8.5). In contrast, τ^0_{off} showed the opposite trend, i.e., shortened with decreasing pH and MEA concentration, e.g., from 623 (10 mM MEA at pH 8.5) to 262 s (10 mM MEA at pH 6.5). This behavior agrees with the previous observation of acid-catalyzed/proton-assisted elimination of the thiol adduct of Cy5.[19] Uncaging of the dark state occurred more efficiently at lower pH, but was also dependent on the thiol concentration, e.g., when reducing the pH at 100 mM MEA τ^0_{off} significantly dropped at pH 6.5, whereas for 10 mM MEA this already occurred at pH 8.0 (Figure 2c).

The ratio of τ_{off} and τ_{on} values were calculated for each subregion in the field of view and for all buffer conditions (Figures 1 and S4). τ_{off}/τ_{on} is a meaningful parameter to determine the maximum achievable resolution with high values indicating the potential to resolve more complex structures with high label densities.[14,22,44] This ratio is inversely linked to the duty cycle ($DC = \tau_{on}/(\tau_{on} + \tau_{off}) \approx (\tau_{off}/\tau_{on})^{-1}$) that has also been used as a metric to characterize the photoswitching performance in SMLM.[12] There are two competing effects that affect the τ_{off}/τ_{on} ratio when varying the intensity. On one hand, an increase of the laser intensity will shorten τ_{on}, which will be beneficial for the τ_{off}/τ_{on} ratio. On the other hand, the sensitivity of k_{on} to the excitation laser as shown in Figure 2b will shorten τ_{off}, which is adversely affecting τ_{off}/τ_{on}. As shown in Figures 1 and S4a, there is a clear trend toward high τ_{off}/τ_{on} ratios for increasing pH and MEA concentrations. τ_{off}/τ_{on} increased through buffer adjustment by 1 order of magnitude from 460 (10 mM MEA at pH 6.5) to 4,600 (100 mM MEA at pH 8.5) (Figure S4a).

Thiolate as Unique Means to Adjust Single-Molecule Photoswitching. Next, we studied key photoswitching metrics as a function of the thiolate (RS^-) concentration, which has been identified as major compound in regulating photoswitching in organic dyes.[10,13,19] To determine the amount of thiolate the pK_a of the thiol group of MEA needs to be known, i.e., the pH at which half of all thiols are deprotonated. Therefore, we titrated MEA in the final switching buffer, i.e., with glucose and enzymatic scavenger system (Figure S5), and determined the pK_a of the thiol group to 8.353 ± 0.004, which agrees with published values.[45,46] Using pH values of 6.5, 7.4, 8.0, and 8.5, the fractions of thiolate could then be calculated to 1.4, 10.0, 30.7, and 58.4% of the applied MEA concentrations, respectively, resulting in

https://doi.org/10.1021/acs.jpcb.2c06872
J. Phys. Chem. B XXXX, XXX, XXX−XXX

thiolate concentrations from 0.14 to 58.4 mM as summarized in Table S1.

As shown in Figure 3a, the photon budget, $N_{\tau on}$, decreased with increasing thiolate concentration, which is due to singlet state quenching and increased dark state formation.[10,19] τ^0_{off} slightly increased toward ~5 mM, then started to significantly increase and finally appeared to saturate >20 mM RS^- (Figure 3b). Interestingly, not only the pH but also the total amount of thiolate seemed to affect the thermal stability of the dark state (cf. Figure 2c), underlining the complexity of the involved thiol chemistry. The sensitivity of the recovery rate to the irradiation intensity was extracted from the gradients of the linear fits as shown in Figure 2b. Here, a strong response of k_{on} could be observed for thiol concentrations <1 mM, with a 4-fold higher sensitivity at ~0.14 mM RS^- (10 mM MEA) when compared to ~1.38 mM RS^- (100 mM MEA), although the pH was still 6.5 (Figure 3c). From 1 mM RS^- onward, the intensity driven response of k_{on} seemed to reach saturation. Although further research is necessary, this finding underlines the importance of a minimum concentration of thiolate to maintain long off-times during imaging at higher intensities. The τ_{off}/τ_{on} ratio on the other hand showed an inverse dependence on the thiolate concentration when compared with $N_{\tau on}$ (Figure 3d). Overall, there seemed to exist no significant difference for τ_{off}/τ_{on} and $N_{\tau on}$, regardless whether high MEA concentrations at low pH or low MEA concentrations at high pH were used as long as the thiolate concentration remained the same, e.g., 250 mM MEA at pH 6.5 and 10 mM MEA at pH 8.0 with ~3.5 and ~3.1 mM RS^-, respectively (Figure 3).

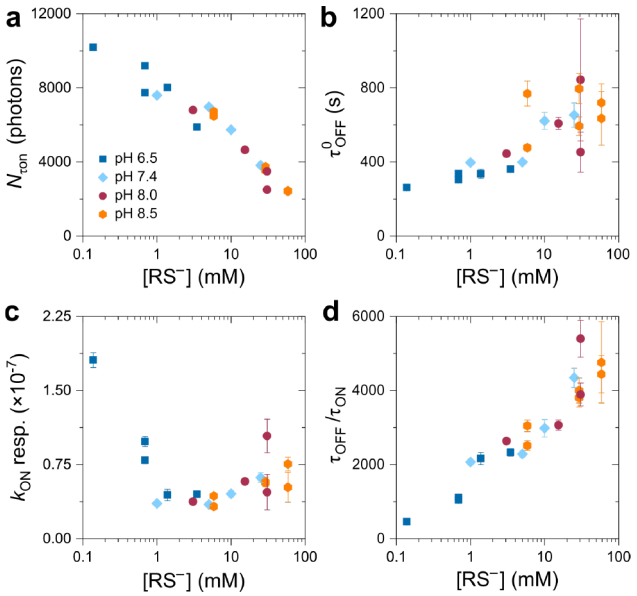

Figure 3. Photoswitching metrics as a function of the thiolate concentration. a) The photon budget per on-state $N_{\tau on}$, b) thermal dark state lifetime τ^0_{off}, c) the intensity response of k_{on} as determined from the gradient of the linear fit as shown in Figure 2, and d) the maximum τ_{off}/τ_{on} ratio (central FOV). The different pH values are indicated by color and symbol. The concentration of thiolate was calculated according to eq 1 using the experimentally determined pK_a of 8.353. Error bars are standard errors from data fits.

In SMLM and tracking experiments, it is desirable to obtain high photon numbers per on-state, to allow for high localization precision.[7,47] On the other hand, the τ_{off}/τ_{on} ratio should be as high as possible, which ensures that only single, isolated spots are localized in a densely labeled sample.[14,44] This trade off needs to be addressed by the buffer composition. Plotting both trends allowed us to identify a range for the optimal thiolate concentration (Figure 4a) where a good photon yield and photoswitching performance can be expected, i.e., >1 mM RS^- with τ_{off}/τ_{on} > 2,000 and $N_{\tau on}$ > 4,000 photons.

To make these two main parameters directly comparable, we calculated the corresponding resolution (Figure 4b). This was done on the basis of the localization precision[36] and on the maximum tolerable label density based on the Nyquist criterion, which states that the sampling interval must be at least twice as fine as the desired resolution.[37] Here, the ability of the localization algorithm to cope with higher spot densities affects the achievable Nyquist resolution, as the localization performance can vary among different software available.[38] For instance, for a label density of 2,500 μm^{-2} (equivalent to 40 nm 2D Nyquist-limited resolution), it makes a difference whether a localization algorithm can handle 1 or 5 spots μm^{-2} (Figure 4b). In the former case τ_{off}/τ_{on} must be at least 2,500 to ensure that one fluorophore on average will be fluorescent,[5]

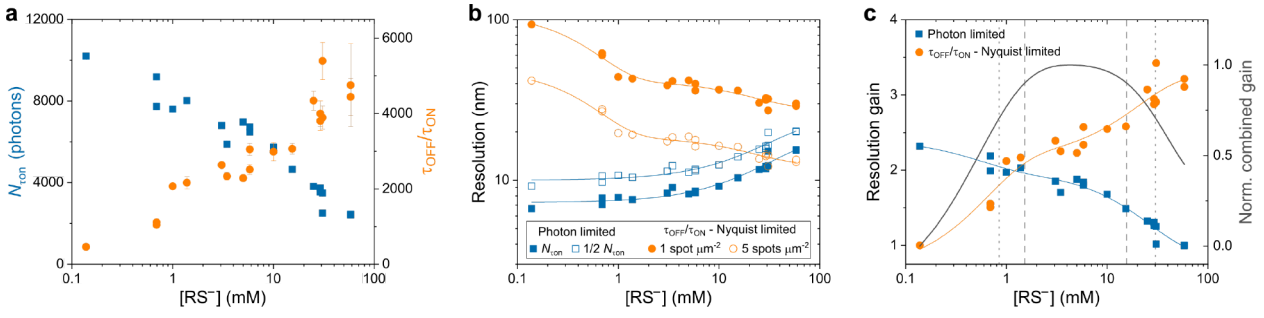

Figure 4. Thiolate driven achievable resolution. a) $N_{\tau on}$ and τ_{off}/τ_{on} as a function of the thiolate concentration. b) Optical resolution calculated from the number of detected photons according to eq 2 (squares) and Nyquist-limited structural 2D resolution calculated from the experimental highest achievable τ_{off}/τ_{on} according to eq 3 (circles). Filled squares refer to resolution determination with $N = N_{\tau on}$; unfilled squares refer to $N = \frac{1}{2}N_{\tau on}$. Filled orange circles refer to a label density $n = \tau_{off}/\tau_{on}$; unfilled circles refer to $n = 5 \times \tau_{off}/\tau_{on}$ per μm^2. Blue and orange solid lines indicate single and double exponential functions fit to the data, respectively. c) Gain in resolution as determined by photon number (squares) and label density (circles). Solid colored lines indicate double exponential functions fit to the data. Curve in dark gray refers to the normalized combined gain in resolution. Dotted and dashed lines in gray indicate concentration bandwidths of 0.85 and 30.15 mM (70.7% combined gain) as well as 1.5 and 15.6 mM RS^- (90%), respectively.

https://doi.org/10.1021/acs.jpcb.2c06872
J. Phys. Chem. B XXXX, XXX, XXX−XXX

whereas in the latter τ_{off}/τ_{on} can be reduced by a factor of 5. In order to apply the Nyquist-Shannon sampling theorem to SMLM, the stochastic nature of sampling further demands an increase of the localization density,[48] which underscores the importance of the τ_{off}/τ_{on} ratio as well as the demand for robust and reliable high density localization algorithms.[38] However, it has been recently demonstrated that for small interfluorophore distances, i.e., <10 nm, resonance energy transfers between adjacent photoswitchable dyes can lead to an increase of activation rates and thus shorten the off-times.[49] For extreme cases, increasing the structural resolution through higher label densities can thus compromise the ability to resolve these.

As shown in Figure 4b, the theoretical resolution based on the available photon budget exceeded the achievable Nyquist-limited resolution. In this case the photon based resolution, which can be considered as the lower bound for the maximum achievable resolution in SMLM, remained relatively constant for thiolate concentrations <10 mM. Above this concentration this resolution significantly decreased due to thiolate induced singlet state quenching of AF647. It should be noted though that even at a thiolate concentration of 20 mM the photon number was still high enough to allow a theoretical resolution of <15 nm. This is opposite to the Nyquist resolution which increased significantly with concentrations toward 1 mM RS^-, after which a further increase can be observed but at a smaller rate.

The effect of thiolate on the photon based resolution can be considered as low pass filter, excluding high thiolate concentrations as the emitter brightness is reduced. On the other hand, its effect on the τ_{off}/τ_{on} limited Nyquist resolution can be described as long pass filter, excluding low thiolate concentrations for which high emitter densities become unresolvable. In order to evaluate the optimal thiolate concentration range, we calculated the gain in resolution from both filters (Figure 4c). The lowest and highest thiolate concentration of the resulting pass band were about ∼1 and 30 mM, respectively. Below and above this bandwidth, the benefit of one parameter is impaired by the other. Within a working concentration range of 1.5−15.6 mM RS^-, photoswitching leads to overall high combined resolution comprising an optimal range of 2.5 and 8.3 mM (Figure S6). The maximum gain at 4.3 mM could be realized with 43 mM MEA at pH 7.4. At this pH the fraction of thiolate is 10% of the employed MEA concentration and thus allows for tuning the thiolate concentration conveniently within the concentration bandwidth. Table 1 and Figure S6d summarize the photoswitching performance of AF647 with MEA.

Table 1. Optimal Buffer Conditions Used in This Study for the Carbocyanine Dye AF647[a]

	pH			
[MEA] (mM)	6.5	7.4	8.0	8.5
10	−	○	+	+
50	−	+	+	○
100	○	+	−	−
250	+	○		

[a]Performance was rated with + (very good), ○ (decent), and − (bad). For conditions rated +, the buffer contained between 1.5 and 15.6 mM RS^- (cf. Figure S6).

Buffers in SMLM experiments should hence be prepared to realize the major gain in structural resolution while avoiding a significant loss of localization precision. With the τ_{off}/τ_{on} ratio as the main limitation to resolve densely labeled structures, it therefore makes sense to exceed the minimum thiolate concentration of 1 mM. If the structural complexity, however, is low, then the thiolate concentration might be reduced to ≤1 mM to allow for high localization precision and fast data acquisition (Figures 3 and 4). On the other hand, buffers with low thiolate concentrations could be advantageously used for imaging complex structures with super-resolution techniques that rely on the temporal analysis of intensity fluctuations such as in SOFI[50] or SRRF.[51]

Acidification of the Enzymatic Oxygen Scavenger System. The oxygen scavenger system applied in this study was based on glucose oxidase and catalase (GOC), which catalyzes the reaction of D-glucose and oxygen to gluconic acid.[52] It is a well-established system for single-molecule experiments in aqueous environment, which facilitates efficient depletion of oxygen within seconds.[33] Accumulation of gluconic acid over time, however, results in acidification of the solvent if oxygen can redissolve from the headspace.[53] This has motivated the development of alternative systems such as substituting glucose oxidase with pyranose oxidase.[54]

Here, we investigated the photoswitching of AF647 over prolonged time periods. Because a pH drop over time would affect the photoswitching performance due to a reduction of the thiolate concentration, we imaged a single-molecule surface in steps of 2 h after preparing the buffer (50 mM MEA, pH 7.4) and left the chamber unsealed. We measured an increase of τ_{on} within 4 h from 161 (0 h) to 183 (2 h) and 224 ms (4 h), while τ_{off} decreased from 169 (0 h) to 97 (2 h) and 55 s (4 h) due to proton-assisted restoration of the ground state of AF647; the pH dropped by ∼1 every 2 h (Figure 5, left). Here, the acidification of the GOC system was slower than

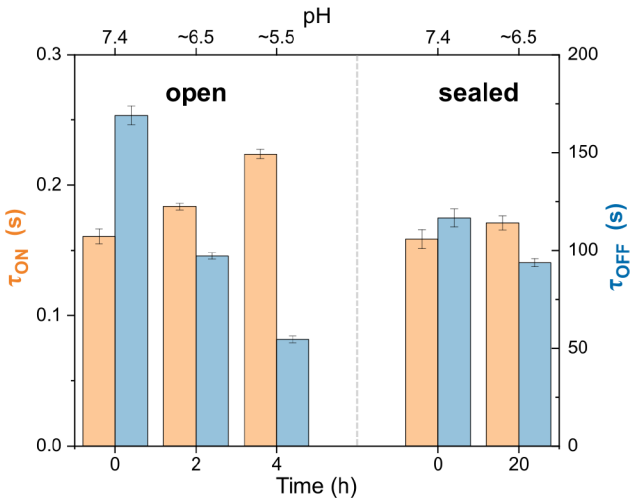

Figure 5. Evaluating the stability of the photoswitching buffer (50 mM MEA, pH 7.4, glucose, glucose oxidase, and catalase system) in sealed and unsealed sample chambers. τ_{on} (orange) and τ_{off} (blue) were determined for each measurement. Left: unsealed LabTek chamber imaged just after adding the buffer (0 h, pH 7.4), 2 h (pH ∼ 6.5) and 4 h (pH ∼ 5.5) afterward; right: completely filled and sealed LabTek chamber just after adding the buffer (0 h, pH 7.4) and 20 h afterward (pH ∼ 6.5). Measurements were performed with flat-field illumination. Error bars are standard errors from data fits.

https://doi.org/10.1021/acs.jpcb.2c06872
J. Phys. Chem. B XXXX, XXX, XXX−XXX

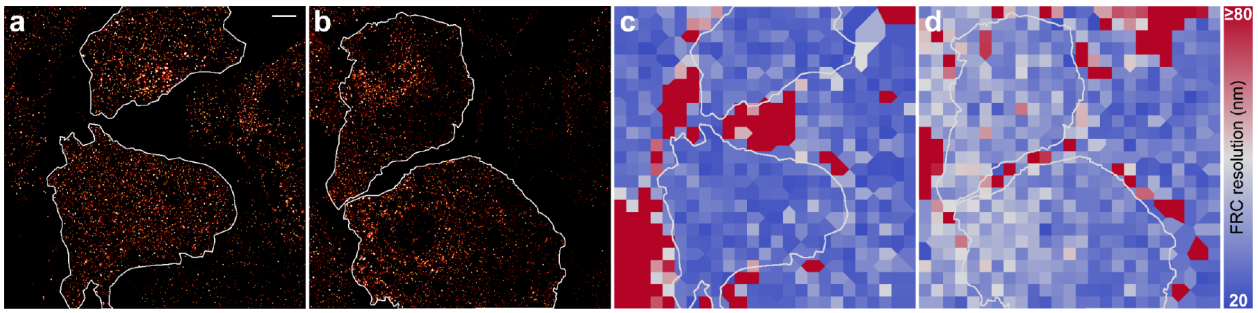

Figure 6. SMLM imaging of GLUT4 in the basal membrane. dSTORM images applying a) 100 mM MEA at pH 7.4 and b) 100 mM MEA at pH 8.0 employing the GOC system. Two cells for each condition were selected and analyzed as shown as white marking. c, d) Corresponding FRC maps with the color code set to FRC resolutions between 20 and ≥80 nm. The FRC resolution was determined to c) 26.1 ± 3.1 (median ± MAD, top cell) and 26.4 ± 2.8 nm (bottom cell), and d) 35.1 ± 4.3 (top cell) and 32.8 ± 5.0 nm (bottom cell). The scale bar of 5 μm in a) applies to all images.

previously reported,[54] which can be explained by the presence of MEA with its main buffering capacity around pH 8.35.

If the reaction chamber was completely filled with photoswitching buffer and sealed on top with a glass coverslip to avoid any headspace for gas exchange, then acidification could be dramatically reduced as shown in Figure 5 (right). τ_{on} and τ_{off} changed by 8% and −20% after an incubation time of 20 h at room temperature, which is significantly lower compared to the unsealed chamber (39% and −68%, respectively, after 4 h). The pH was measured to drop by ∼1 within 20 h, thus the stability was increased by at least 1 order of magnitude. Our results agree with the findings employing GOC with 143 mM BME at pH 8 where single-molecule brightness and localization density were studied in chambers sealed with parafilm.[41] pH stability could be further increased by increasing the buffering capacity of the thiol compound, which can be achieved by increasing the thiol concentration or setting the pH toward the pK_a.

Single-molecule photoswitching has also been demonstrated using solely MEA at moderate alkaline pH in aqueous environment.[10,14,55] Besides its photoswitching capability, it has further been demonstrated that MEA solutions also act as efficient oxygen scavenger although at depletion rates lower than the GOC system.[33] We therefore used our approach to compare photoswitching of AF647 in presence and absence of GOC (Figure S7). Both $N_{\tau on}$ and τ_{off}/τ_{on} are moderately improved by using GOC for the optimal thiolate concentration as determined in this work, thus its use in SMLM is generally advisable. However, the use of a buffer with mere thiol can be beneficial for applications where the photoswitching buffer should be designed as simple as possible, e.g., spectroscopic measurements[13] and correlative microscopy approaches where SMLM is combined with atomic force microscopy[55] or expansion microscopy.[56]

Consequences for Biological Imaging. To demonstrate the impact on minor changes of the pH in biological imaging, we imaged the glucose transporter GLUT4 in the basal membrane of adipocyte cells in flat-field illumination with 100 mM MEA (Figure 6). To assess the overall SMLM image quality, we determined the resolution by Fourier ring correlation (FRC),[35] which was calculated to 26 ± 3 and 34 ± 5 nm (median ± MAD) for pH 7.4 and 8.0, respectively. The decrease in FRC resolution can be explained with a reduced amount in localizations from a density of ∼1,740 to ∼560 localizations μm^{-2}. Consequently, GLUT4 should be imaged at pH 7.4 under the experimental settings. The corresponding thiolate concentration of 10 mM is within the proposed concentration range and allows for imaging at high τ_{off}/τ_{on} ratio, whereas an increase of the pH by 0.6 to pH 8.0 exceeds the thiolate concentration by a factor of 3 (∼31 mM) with an overall detrimental effect on the resolution.

The resolution as determined by FRC could be increased for higher pH values by increasing the acquisition length to gain more localizations. Alternatively, additional activation at shorter wavelength could be used.[16,17,19] On the other hand, the increased τ_{off}/τ_{on} ratio for pH 8.0 allowed for imaging with a reduced amount of artifacts, but whether the label density demands this ratio is questionable. The τ_{off}/τ_{on} ratio always sets a limit for the maximum achievable resolution, but it should ideally fit the label density to not waste acquisition time. This is, however, technically challenging without a priori knowledge of the label density.

In summary, for achieving the highest possible resolution the thiolate concentration should be kept as low as possible to gain high photon budgets and the maximum amount of localizations. It is advisable to adapt the thiolate concentration a posteriori, e.g., if artifacts are detected.[35] To minimize artifacts from the very start, thiolate can be used at higher concentrations, but this can come at the cost of an overall reduced resolution.

CONCLUSIONS

Controlling the photoswitching performance is key for the successful implementation of SMLM in quantitative biology. Therefore, the right adjustment of the chemical buffer composition is of utmost importance. By means of a MEMS micromirror, we studied single carbocyanine dye molecules at varying intensities within a single acquisition and by using an automated workflow we determined key photoswitching metrics such as spot brightness, N_{Det}, the fluorescent on-state lifetime, τ_{on}, and off-state lifetime, τ_{off}, for a range of different buffer settings. The performance of photoswitching was linked to the thiolate concentration, which is defined by the concentration of the thiol such as MEA and the pH of the solvent.

Thiolate was characterized to have a concentration bandwidth in the range of 1−16 mM, which allows for achieving high resolution through molecular brightness and τ_{off}/τ_{on} ratio. This range allows for tailoring carbocyanine photoswitching to SMLM imaging needs. Reducing the thiolate concentration will enhance molecular brightness, whereas an increase shortens τ_{on}, improves the longevity of

https://doi.org/10.1021/acs.jpcb.2c06872
J. Phys. Chem. B XXXX, XXX, XXX−XXX

τ_{off} and thus the duty cycle. A good starting point when imaging unknown structures will be 50 mM MEA at pH 7.4 or 10 mM MEA at pH 8.0 with ∼5.0 and ∼3.1 mM thiolate, respectively. The optimal thiolate concentration for cyanine photoswitching can be realized at different pH values (Figure 3). This will allow for setting the pH toward levels that are facilitating other chemical processes in the sample, e.g., enzymatic activity or the simultaneous use of dyes with pH dependent blinking.[57,58] Although suboptimal for SMLM, minimal thiolate concentrations can be interesting for super-resolution methods based on the temporal analysis of intensity fluctuations.[50,51]

For a comparison of different thiol containing reducing agents the corresponding thiolate concentration needs to be taken into account. Besides MEA, BME is frequently used for photoswitching of organic dyes,[12,19,41] typically at concentrations of 1%, i.e., 143 mM at pH 8.0. With a pK_a of 9.6 for BME[59] the corresponding thiolate concentration can be calculated to ∼3.5 mM, which is comparable with the aforementioned MEA concentrations. However, the thiolate concentration can only be calculated using a precise estimate of the pK_a of the thiol group, and a range of values has been published owing to different measurement techniques and experimental conditions, e.g., between 8.19 and 8.6 for MEA[60,61] and 9.5 and 9.8 for BME[61,62] (Table S2). Small deviations among these values can render an estimation of the exact amount of thiolate challenging, e.g., with ∼2.4-fold more thiolate at pH 7.4 when using 8.19 instead of 8.6 as pK_a for MEA (cf. Figure S8). As such, a titration of the employed thiol in the final experimental buffer environment is advisable. This also underpins the importance of indicating pH and buffer conditions in photoswitching experiments.

Acidification of the popular oxygen scavenger system employing glucose, glucose oxidase, and catalase has been investigated in several studies.[41,53,54,63] Here, we demonstrated that sealing of the reaction chamber without leaving air headspace is the most critical measure to avoid a significant pH drop with GOC over time. By monitoring τ_{on} and τ_{off} over time AF647 has been used as a sensor for the pH change. By proper sealing, e.g., by using a coverslip on top of a fully filled imaging chamber, consistent photoswitching can be performed for several hours without significant pH drop even with the GOC system. Alternative oxygen scavenger systems without being prone to acidification can hold the pH, but if the imaging chamber remains unsealed the chemical composition will change over time due to the ongoing influx of oxygen.

Ultimately, the perfect buffer composition will depend on the structural complexity in SMLM experiments. High τ_{off}/τ_{on} ratios are needed when the label density increases, which can be the case for biological samples with a natural variability in protein expression. Therefore, a perfusion system could advantageously be used to adapt the amount of thiolate on the fly,[64] i.e., through changing pH or thiol concentration.

■ ASSOCIATED CONTENT

Supporting Information

The Supporting Information is available free of charge at https://pubs.acs.org/doi/10.1021/acs.jpcb.2c06872.

Photoswitching analysis, MEA titration, thiolate concentration and SMLM resolution, performance of MEA without enzymatic oxygen scavenger system, thiolate fraction by pK_a values (PDF)

■ AUTHOR INFORMATION

Corresponding Author

Sebastian van de Linde − *Department of Physics, SUPA, University of Strathclyde, Glasgow G4 0NG Scotland, United Kingdom*; orcid.org/0000-0002-7977-840X; Email: s.vandelinde@strath.ac.uk

Authors

Lucas Herdly − *Department of Physics, SUPA, University of Strathclyde, Glasgow G4 0NG Scotland, United Kingdom*

Peter W. Tinning − *Department of Physics, SUPA, University of Strathclyde, Glasgow G4 0NG Scotland, United Kingdom*

Angéline Geiser − *Strathclyde Institute of Pharmacy and Biomedical Sciences, University of Strathclyde, Glasgow G4 0RE Scotland, United Kingdom*; orcid.org/0000-0002-7108-2440

Holly Taylor − *Strathclyde Institute of Pharmacy and Biomedical Sciences, University of Strathclyde, Glasgow G4 0RE Scotland, United Kingdom*

Gwyn W. Gould − *Strathclyde Institute of Pharmacy and Biomedical Sciences, University of Strathclyde, Glasgow G4 0RE Scotland, United Kingdom*

Complete contact information is available at: https://pubs.acs.org/10.1021/acs.jpcb.2c06872

Notes

The authors declare no competing financial interest.

■ ACKNOWLEDGMENTS

We are grateful to Ralf Bauer and Paul Janin (University of Strathclyde, Glasgow) for providing us with the MEMS mirror. This work was supported by the EPSRC (EP/V048031/1) and the Academy of Medical Sciences/the British Heart Foundation/the Government Department of Business, Energy and Industrial Strategy/the Wellcome Trust Springboard Award (SBF003\1163). L.H. was supported by doctoral fellowships (EPSRC studentship 2031229 and EPSRC Doctoral Training Partnership (DTP) grant EP/N509760/1). H.T. was supported by a Studentship from Diabetes UK (18/0005905), and A.G. was supported by a studentship from EPSRC (EP/T517938/1). Data supporting the findings of this study are available from the authors upon reasonable request.

■ REFERENCES

(1) Sauer, M.; Heilemann, M. Single-Molecule Localization Microscopy in Eukaryotes. *Chem. Rev.* **2017**, *117*, 7478−7509.

(2) Vangindertael, J.; Camacho, R.; Sempels, W.; Mizuno, H.; Dedecker, P.; Janssen, K. P. F. An introduction to optical super-resolution microscopy for the adventurous biologist. *Methods Appl. Fluoresc.* **2018**, *6*, 022003.

(3) Valli, J.; Garcia-Burgos, A.; Rooney, L. M.; Vale de Melo e Oliveira, B.; Duncan, R. R.; Rickman, C. Seeing beyond the limit: A guide to choosing the right super-resolution microscopy technique. *J. Biol. Chem.* **2021**, *297*, 100791.

(4) Ha, T.; Tinnefeld, P. Photophysics of Fluorescent Probes for Single-Molecule Biophysics and Super-Resolution Imaging. *Annu. Rev. Phys. Chem.* **2012**, *63*, 595−617.

(5) van de Linde, S.; Sauer, M. How to switch a fluorophore: from undesired blinking to controlled photoswitching. *Chem. Soc. Rev.* **2014**, *43*, 1076−1087.

(6) Stennett, E. M. S.; Ciuba, M. A.; Levitus, M. Photophysical processes in single molecule organic fluorescent probes. *Chem. Soc. Rev.* **2014**, *43*, 1057−1075.

(7) Li, H.; Vaughan, J. C. Switchable Fluorophores for Single-Molecule Localization Microscopy. *Chem. Rev.* **2018**, *118*, 9412−9454.
(8) Heilemann, M.; Margeat, E.; Kasper, R.; Sauer, M.; Tinnefeld, P. Carbocyanine Dyes as Efficient Reversible Single-Molecule Optical Switch. *J. Am. Chem. Soc.* **2005**, *127*, 3801−3806.
(9) Bates, M.; Blosser, T. R.; Zhuang, X. Short-range spectroscopic ruler based on a single-molecule optical switch. *Phys. Rev. Lett.* **2005**, *94*, 108101.
(10) Heilemann, M.; van de Linde, S.; Mukherjee, A.; Sauer, M. Super-Resolution Imaging with Small Organic Fluorophores. *Angew. Chem., Int. Ed.* **2009**, *48*, 6903−6908.
(11) Vogelsang, J.; Cordes, T.; Forthmann, C.; Steinhauer, C.; Tinnefeld, P. Controlling the fluorescence of ordinary oxazine dyes for single-molecule switching and superresolution microscopy. *Proc. Natl. Acad. Sci. U.S.A.* **2009**, *106*, 8107−8112.
(12) Dempsey, G. T.; Vaughan, J. C.; Chen, K. H.; Bates, M.; Zhuang, X. Evaluation of fluorophores for optimal performance in localization-based super-resolution imaging. *Nat. Methods* **2011**, *8*, 1027−36.
(13) van de Linde, S.; Krstić, I.; Prisner, T.; Doose, S.; Heilemann, M.; Sauer, M. Photoinduced formation of reversible dye radicals and their impact on super-resolution imaging. *Photochem. Photobiol. Sci.* **2011**, *10*, 499−506.
(14) van de Linde, S.; Löschberger, A.; Klein, T.; Heidbreder, M.; Wolter, S.; Heilemann, M.; Sauer, M. Direct stochastic optical reconstruction microscopy with standard fluorescent probes. *Nat. Protoc.* **2011**, *6*, 991−1009.
(15) Rust, M. J.; Bates, M.; Zhuang, X. W. Sub-diffraction-limit imaging by stochastic optical reconstruction microscopy (STORM). *Nat. Methods* **2006**, *3*, 793−795.
(16) Heilemann, M.; van de Linde, S.; Schüttpelz, M.; Kasper, R.; Seefeldt, B.; Mukherjee, A.; Tinnefeld, P.; Sauer, M. Subdiffraction-resolution fluorescence imaging with conventional fluorescent probes. *Angew. Chem., Int. Ed. Engl.* **2008**, *47*, 6172−6.
(17) Dempsey, G. T.; Bates, M.; Kowtoniuk, W. E.; Liu, D. R.; Tsien, R. Y.; Zhuang, X. Photoswitching Mechanism of Cyanine Dyes. *J. Am. Chem. Soc.* **2009**, *131*, 18192−18193.
(18) Holzmeister, P.; Gietl, A.; Tinnefeld, P. Geminate Recombination as a Photoprotection Mechanism for Fluorescent Dyes. *Angew. Chem., Int. Ed.* **2014**, *53*, 5685−5688.
(19) Gidi, Y.; Payne, L.; Glembockyte, V.; Michie, M. S.; Schnermann, M. J.; Cosa, G. Unifying Mechanism for Thiol-Induced Photoswitching and Photostability of Cyanine Dyes. *J. Am. Chem. Soc.* **2020**, *142*, 12681−12689.
(20) Thompson, R. E.; Larson, D. R.; Webb, W. W. Precise nanometer localization analysis for individual fluorescent probes. *Biophys. J.* **2002**, *82*, 2775−83.
(21) Mau, A.; Friedl, K.; Leterrier, C.; Bourg, N.; Lévêque-Fort, S. Fast widefield scan provides tunable and uniform illumination optimizing super-resolution microscopy on large fields. *Nat. Commun.* **2021**, *12*, 3077.
(22) Herdly, L.; Janin, P.; Bauer, R.; van de Linde, S. Tunable Wide-Field Illumination and Single-Molecule Photoswitching with a Single MEMS Mirror. *ACS Photonics* **2021**, *8*, 2728−2736.
(23) Klip, A.; McGraw, T. E.; James, D. E. Thirty sweet years of GLUT4. *J. Biol. Chem.* **2019**, *294*, 11369−11381.
(24) Stenkula, K. G.; Lizunov, V. A.; Cushman, S. W.; Zimmerberg, J. Insulin controls the spatial distribution of GLUT4 on the cell surface through regulation of its postfusion dispersal. *Cell Metab.* **2010**, *12*, 250−259.
(25) Lizunov, V. A.; Stenkula, K.; Troy, A.; Cushman, S. W.; Zimmerberg, J. Insulin regulates Glut4 confinement in plasma membrane clusters in adipose cells. *PLoS One* **2013**, *8*, e57559.
(26) Gao, L.; Chen, J.; Gao, J.; Wang, H.; Xiong, W. Super-resolution microscopy reveals the insulin-resistance-regulated reorganization of GLUT4 on plasma membranes. *J. Cell Sci.* **2016**, *130*, 396−405.
(27) Koester, A. M.; Geiser, A.; Laidlaw, K. M. E.; Morris, S.; Cutiongco, M. F. A.; Stirrat, L.; Gadegaard, N.; Boles, E.; Black, H. L.; Bryant, N. J. EFR3 and phosphatidylinositol 4-kinase IIIα regulate insulin-stimulated glucose transport and GLUT4 dispersal in 3T3-L1 adipocytes. *Biosci. Rep.* **2022**, *42*, BSR20221181.
(28) Schindelin, J.; Arganda-Carreras, I.; Frise, E.; Kaynig, V.; Longair, M.; Pietzsch, T.; Preibisch, S.; Rueden, C.; Saalfeld, S.; Schmid, B.; et al. Fiji: an open-source platform for biological-image analysis. *Nat. Methods* **2012**, *9*, 676−82.
(29) van de Linde, S. Single-molecule localization microscopy analysis with ImageJ. *J. Phys. D: Appl. Phys.* **2019**, *52*, 203002.
(30) Morris, S.; Geoghegan, N. D.; Sadler, J. B. A.; Koester, A. M.; Black, H. L.; Laub, M.; Miller, L.; Heffernan, L.; Simpson, J. C.; Mastick, C. C.; et al. Characterisation of GLUT4 trafficking in HeLa cells: comparable kinetics and orthologous trafficking mechanisms to 3T3-L1 adipocytes. *PeerJ.* **2020**, *8*, e8751.
(31) Habtemichael, E. N.; Brewer, P. D.; Romenskaia, I.; Mastick, C. C. Kinetic evidence that Glut4 follows different endocytic pathways than the receptors for transferrin and alpha2-macroglobulin. *J. Biol. Chem.* **2011**, *286*, 10115−10125.
(32) Blot, V.; McGraw, T. E. Use of quantitative immunofluorescence microscopy to study intracellular trafficking: studies of the GLUT4 glucose transporter. *Methods Mol. Biol.* **2008**, *457*, 347−366.
(33) Schäfer, P.; van de Linde, S.; Lehmann, J.; Sauer, M.; Doose, S. Methylene blue- and thiol-based oxygen depletion for super-resolution imaging. *Anal. Chem.* **2013**, *85*, 3393−400.
(34) Burner, U.; Obinger, C. Transient-state and steady-state kinetics of the oxidation of aliphatic and aromatic thiols by horseradish peroxidase. *FEBS Lett.* **1997**, *411*, 269−274.
(35) Culley, S.; Albrecht, D.; Jacobs, C.; Pereira, P. M.; Leterrier, C.; Mercer, J.; Henriques, R. Quantitative mapping and minimization of super-resolution optical imaging artifacts. *Nat. Methods* **2018**, *15*, 263−266.
(36) Mortensen, K. I.; Churchman, L. S.; Spudich, J. A.; Flyvbjerg, H. Optimized localization analysis for single-molecule tracking and super-resolution microscopy. *Nat. Methods* **2010**, *7*, 377−81.
(37) Shroff, H.; Galbraith, C. G.; Galbraith, J. A.; Betzig, E. Live-cell photoactivated localization microscopy of nanoscale adhesion dynamics. *Nat. Methods* **2008**, *5*, 417−423.
(38) Sage, D.; Pham, T.-A.; Babcock, H.; Lukes, T.; Pengo, T.; Chao, J.; Velmurugan, R.; Herbert, A.; Agrawal, A.; Colabrese, S.; et al. Super-resolution fight club: assessment of 2D and 3D single-molecule localization microscopy software. *Nat. Methods* **2019**, *16*, 387−395.
(39) Eggeling, C.; Widengren, J.; Rigler, R.; Seidel, C. A. M. Photobleaching of Fluorescent Dyes under Conditions Used for Single-Molecule Detection: Evidence of Two-Step Photolysis. *Anal. Chem.* **1998**, *70*, 2651−9.
(40) Dittrich, P. S.; Schwille, P. Photobleaching and stabilization of fluorophores used for single-molecule analysis with one- and two-photon excitation. *Appl. Phys. B: Laser Opt.* **2001**, *73*, 829−837.
(41) Diekmann, R.; Kahnwald, M.; Schoenit, A.; Deschamps, J.; Matti, U.; Ries, J. Optimizing imaging speed and excitation intensity for single-molecule localization microscopy. *Nat. Methods* **2020**, *17*, 909−912.
(42) Chung, J.; Jeong, U.; Jeong, D.; Go, S.; Kim, D. Development of a New Approach for Low-Laser-Power Super-Resolution Fluorescence Imaging. *Anal. Chem.* **2022**, *94*, 618−627.
(43) Steinhauer, C.; Forthmann, C.; Vogelsang, J.; Tinnefeld, P. Superresolution Microscopy on the Basis of Engineered Dark States. *J. Am. Chem. Soc.* **2008**, *130*, 16840−16841.
(44) Cordes, T.; Strackharn, M.; Stahl, S. W.; Summerer, W.; Steinhauer, C.; Forthmann, C.; Puchner, E. M.; Vogelsang, J.; Gaub, H. E.; Tinnefeld, P. Resolving single-molecule assembled patterns with superresolution blink-microscopy. *Nano Lett.* **2010**, *10*, 645−51.
(45) Li, N. C.; Manning, R. A. Some Metal Complexes of Sulfur-containing Amino Acids. *J. Am. Chem. Soc.* **1955**, *77*, 5225−5228.

https://doi.org/10.1021/acs.jpcb.2c06872
J. Phys. Chem. B XXXX, XXX, XXX−XXX

(46) Benesch, R. E.; Benesch, R. The Acid Strength of the -SH Group in Cysteine and Related Compounds. *J. Am. Chem. Soc.* **1955**, *77*, 5877−5881.
(47) Shen, H.; Tauzin, L. J.; Baiyasi, R.; Wang, W.; Moringo, N.; Shuang, B.; Landes, C. F. Single Particle Tracking: From Theory to Biophysical Applications. *Chem. Rev.* **2017**, *117*, 7331−7376.
(48) Legant, W. R.; Shao, L.; Grimm, J. B.; Brown, T. A.; Milkie, D. E.; Avants, B. B.; Lavis, L. D.; Betzig, E. High-density three-dimensional localization microscopy across large volumes. *Nat. Methods* **2016**, *13*, 359−365.
(49) Helmerich, D. A.; Beliu, G.; Taban, D.; Meub, M.; Streit, M.; Kuhlemann, A.; Doose, S.; Sauer, M. Photoswitching fingerprint analysis bypasses the 10-nm resolution barrier. *Nat. Methods* **2022**, *19*, 986−994.
(50) Dertinger, T.; Colyer, R.; Iyer, G.; Weiss, S.; Enderlein, J. Fast, background-free, 3D super-resolution optical fluctuation imaging (SOFI). *Proc. Natl. Acad. Sci. U.S.A.* **2009**, *106*, 22287−22292.
(51) Gustafsson, N.; Culley, S.; Ashdown, G.; Owen, D. M.; Pereira, P. M.; Henriques, R. Fast live-cell conventional fluorophore nanoscopy with ImageJ through super-resolution radial fluctuations. *Nat. Commun.* **2016**, *7*, 12471.
(52) Benesch, R. E.; Benesch, R. Enzymatic Removal of Oxygen for Polarography and Related Methods. *Science* **1953**, *118*, 447−448.
(53) Shi, X.; Lim, J.; Ha, T. Acidification of the Oxygen Scavenging System in Single-Molecule Fluorescence Studies: In Situ Sensing with a Ratiometric Dual-Emission Probe. *Anal. Chem.* **2010**, *82*, 6132−6138.
(54) Swoboda, M.; Henig, J.; Cheng, H.-M.; Brugger, D.; Haltrich, D.; Plumeré, N.; Schlierf, M. Enzymatic Oxygen Scavenging for Photostability without pH Drop in Single-Molecule Experiments. *ACS Nano* **2012**, *6*, 6364−6369.
(55) Hirvonen, L. M.; Cox, S. STORM without enzymatic oxygen scavenging for correlative atomic force and fluorescence super-resolution microscopy. *Methods Appl. Fluoresc.* **2018**, *6*, 045002.
(56) Zwettler, F. U.; Reinhard, S.; Gambarotto, D.; Bell, T. D. M.; Hamel, V.; Guichard, P.; Sauer, M. Molecular resolution imaging by post-labeling expansion single-molecule localization microscopy (Ex-SMLM). *Nat. Commun.* **2020**, *11*, 3388.
(57) Uno, S.-N.; Kamiya, M.; Yoshihara, T.; Sugawara, K.; Okabe, K.; Tarhan, M. C.; Fujita, H.; Funatsu, T.; Okada, Y.; Tobita, S.; et al. A spontaneously blinking fluorophore based on intramolecular spirocyclization for live-cell super-resolution imaging. *Nat. Chem.* **2014**, *6*, 681−689.
(58) Macdonald, P. J.; Gayda, S.; Haack, R. A.; Ruan, Q.; Himmelsbach, R. J.; Tetin, S. Y. Rhodamine-Derived Fluorescent Dye with Inherent Blinking Behavior for Super-Resolution Imaging. *Anal. Chem.* **2018**, *90*, 9165−9173.
(59) Jencks, W. P.; Salvesen, K. Equilibrium deuterium isotope effects on the ionization of thiol acids. *J. Am. Chem. Soc.* **1971**, *93*, 4433−4436.
(60) Serjeant, E. P.; Dempsey, B.*Ionisation Constants of Organic Acids in Aqueous Solution*; IUPAC Chemical Data Series, no. 23; Pergamon Press: Oxford; New York, 1979.
(61) Lundblad, R. L., Macdonald, F., Eds. *Handbook of Biochemistry and Molecular Biology*, 5th ed.; CRC Press: Boca Raton, FL, 2018.
(62) Suwandaratne, N.; Hu, J.; Siriwardana, K.; Gadogbe, M.; Zhang, D. Evaluation of Thiol Raman Activities and pKa Values Using Internally Referenced Raman-Based pH Titration. *Anal. Chem.* **2016**, *88*, 3624−3631.
(63) Nahidiazar, L.; Agronskaia, A. V.; Broertjes, J.; van den Broek, B.; Jalink, K. Optimizing Imaging Conditions for Demanding Multi-Color Super Resolution Localization Microscopy. *PLoS One* **2016**, *11*, e0158884.
(64) Almada, P.; Pereira, P. M.; Culley, S.; Caillol, G.; Boroni-Rueda, F.; Dix, C. L.; Charras, G.; Baum, B.; Laine, R. F.; Leterrier, C.; et al. Automating multimodal microscopy with NanoJ-Fluidics. *Nat. Commun.* **2019**, *10*, 1223.

https://doi.org/10.1021/acs.jpcb.2c06872
J. Phys. Chem. B XXXX, XXX, XXX−XXX